Theoretical study on superconductivity in $CeMIn_5$ (M = Co, Rh, Ir): pairing symmetry and pressure dependence

2007 J. Phys.: Condens. Matter 19 406219

(http://iopscience.iop.org/0953-8984/19/40/406219)

IOP PUBLISHING JOURNAL OF PHYSICS: CONDENSED MATTER

J. Phys.: Condens. Matter **19** (2007) 406219 (15pp) doi:10.1088/0953-8984/19/40/406219

Theoretical study on superconductivity in $CeMIn_5$ (M = Co, Rh, Ir): pairing symmetry and pressure dependence

Kazunori Tanaka[1], **Hiroaki Ikeda**[2], **Yunori Nisikawa**[3] **and Kosaku Yamada**[4]

[1] Department of Physics, Faculty of Science and Technology, Tokyo University of Science, Noda 278-8510, Chiba, Japan
[2] Department of Physics, Kyoto University, Kyoto 606-8502, Kyoto, Japan
[3] Department of Material Science, Osaka City University, Osaka 558-8585, Osaka, Japan
[4] Faculty of Science and Engineering, Ritsumeikan University, Kusatsu 525-8577, Siga, Japan

E-mail: ktanaka@ph.noda.tus.ac.jp

Received 8 June 2007, in final form 2 August 2007
Published 12 September 2007
Online at stacks.iop.org/JPhysCM/19/406219

Abstract

We study theoretically heavy fermion superconductors $CeMIn_5$ (M = Co, Rh, Ir). $CeCoIn_5$ and $CeIrIn_5$ that become superconducting at ambient pressure with $T_c = 2.3$ K and 0.4 K, respectively. On the other hand, $CeRhIn_5$ is an antiferromagnet at ambient pressure and becomes superconducting under pressures greater than 1.6 GPa. With regards to the superconductivity, the existence of line nodes is indicated by nuclear-quadrupole-resonance (NQR), thermal conductivity, specific heat and electrical resistivity measurements. However, the pairing symmetry between $d_{x^2-y^2}$ and d_{xy} is controversial. Therefore, we investigate the gap structure of $CeMIn_5$ by a detailed calculation. We introduce a three-dimensional periodic Anderson model (3D-PAM) in order to reproduce the band characteristics of $CeMIn_5$. Thus, we identify the gap structure of $CeMIn_5$ as the $d_{x^2-y^2}$ symmetry by solving the Èliashberg equations. In addition, we discuss the pressure dependence of T_c and show that two factors determine T_c. One factor is the momentum dependence of quasi-particle interaction and the other factor is the wavefunction renormalization factor. Thus, we have explained the superconductivity in $CeMIn_5$ using the Fermi liquid theory.

1. Introduction

We study heavy fermion superconductors $CeMIn_5$ (M = Co, Rh, Ir) with the periodic Anderson model. $CeCoIn_5$ and $CeIrIn_5$ become superconducting at ambient pressure with $T_c = 2.3$ K and 0.4 K, respectively [1, 2]. On the other hand, $CeRhIn_5$ is an antiferromagnet at ambient pressure and is superconducting under pressure $P > 1.6$ GPa [3, 4]. The existence of line

nodes is indicated by nuclear-quadrupole-resonance (NQR) [5–10], thermal conductivity [11], specific heat [1–4, 11, 12] and electrical resistivity [1–3] measurements. However, the pairing symmetry between $d_{x^2-y^2}$ and d_{xy} is controversial. The thermal conductivity [13–18] and specific heat [19] are measured in a rotating magnetic field, in order to identify the pairing symmetry of $CeCoIn_5$. Izawa *et al* assert that the thermal conductivity measurements suggest $d_{x^2-y^2}$ pairing symmetry [13–18]; on the other hand, Aoki *et al* assert that the specific heat measurements suggest d_{xy} symmetry [19]. Therefore, we identify the pairing symmetry of $CeMIn_5$ by a numerical calculation with the use of the Fermi liquid theory.

A similar calculation has already been performed using a two-dimensional (2D) Hubbard model [20, 21]. However, the 2D Hubbard model is insufficient to describe $CeMIn_5$, since the two-dimensionality of the Fermi surface is not very distinct. Therefore, we take into account the three-dimensionality in order to reproduce the band structure obtained from band calculations [22–28]. In order to reproduce these characteristics, we introduce a three-dimensional periodic Anderson model (3D-PAM) [29]. A study of the pairing symmetry in $CeMIn_5$ has already been published [30]. However, several mistakes have been found in that paper. The main mistake is in the calculation of the eigenvalue of the Èliashberg equation for $d_{x^2-y^2}$ and d_{xy} symmetry. To correct these mistakes, we refined the calculation. In this paper, we improve the model by introducing a more appropriate 3D-PAM than that used in the previous paper. As a result, we do not find any essential changes in qualitative behaviour, although some quantitative changes are observed. Moreover, T_c does not increase monotonically with the strength of the electron correlation; T_c may decrease since it also depends on the renormalization factor. This fact explains the pressure dependence of T_c. Thus, in this paper we study the superconductivity in $CeMIn_5$ in detail, in order to identify the superconducting gap structure and to discuss the pressure dependence of T_c [31].

2. Periodic Anderson model for $CeMIn_5$

A 3D-PAM [29, 32] for $CeMIn_5$ is introduced in this section. The band structure of $CeMIn_5$ comprises several f-bands and conduction bands which are hybridized in a complex manner. However, it is quite difficult to reproduce such a complicated band structure. Moreover, the electron correlation among f-electrons is strong and should be distinguished from that among the conduction bands. Thus, for simplicity, we adopt a 3D-PAM which comprises one f-band and one conduction band.

Now we discuss the lattice structure. The lattice structure of $CeMIn_5$ is tetragonal, and a unit cell contains one Ce atom, one M atom and five In atoms. Here, we focus on Ce atoms in the crystal, since Ce atoms provide 4f-electrons. Therefore we assume a simple tetragonal crystal whose corners are occupied by Ce atoms.

First, we separate the self-energy term $\Sigma(\boldsymbol{k}, \omega)$ into the local part $\Sigma_{\rm loc}(\omega)$ and the non-local part $\Delta\Sigma(\boldsymbol{k}, \omega)$ [20]. In principle, this separation is always possible:

$$\Sigma(\boldsymbol{k}, \omega) = \Sigma_{\rm loc}(\omega) + \Delta\Sigma(\boldsymbol{k}, \omega). \tag{1}$$

$\Sigma_{\rm loc}(\omega)$ is the local part of the self-energy term which does not exhibit momentum dependence. In the vicinity of the Fermi surfaces, the f-electron Green's function is expressed as follows [20, 33–35]:

$$\begin{aligned} G(\boldsymbol{k}, \omega) &= \frac{1}{\omega - \varepsilon^{\rm f}_{\boldsymbol{k}0} - \Sigma(\boldsymbol{k}, \omega) - V_{\boldsymbol{k}}^2/\left(\omega - \varepsilon^{\rm c}_{\boldsymbol{k}}\right)} \\ &= \frac{z_0}{\omega - \tilde{E}^{\rm f}_{\boldsymbol{k}} - \tilde{\Sigma}(\boldsymbol{k}, \omega) - \tilde{V}_{\boldsymbol{k}}^2/\left(\omega - \varepsilon^{\rm c}_{\boldsymbol{k}}\right)} + G_{\rm inc}(\boldsymbol{k}, \omega) \\ &= z_0 \tilde{G}(\boldsymbol{k}, \omega) + G_{\rm inc}(\boldsymbol{k}, \omega), \end{aligned} \tag{2}$$

where $z_0 = (1 - \frac{\mathrm{d}\Sigma_{\mathrm{loc}}(\omega=0)}{\mathrm{d}\omega})^{-1}$ is the local wavefunction renormalization factor and does not exhibit momentum dependence. In (2), $\tilde{E}^{\mathrm{f}}_{\boldsymbol{k}} = z_0(\varepsilon^{\mathrm{f}}_{\boldsymbol{k}0} + \mathrm{Re}\,\Sigma_{\mathrm{loc}}(\omega = 0))$, $\tilde{V}_{\boldsymbol{k}} = \sqrt{z_0}V_{\boldsymbol{k}}$, $\tilde{G}(\boldsymbol{k}, \omega)$, $\tilde{\Sigma}(\boldsymbol{k}, \omega) = z_0\Delta\Sigma(\boldsymbol{k}, \omega)$, $\varepsilon^{\mathrm{c}}_{\boldsymbol{k}}$ and $G_{\mathrm{inc}}(\boldsymbol{k}, \omega)$ are the renormalized f-band dispersion, the renormalized hybridization term, the renormalized Green's function, the renormalized non-local self-energy term, the conduction band dispersion and the incoherent part of the Green's function, respectively. Equation (2) indicates that heavy fermion systems are described with the f-band dispersion and the hybridization term renormalized by z_0 and by $\sqrt{z_0}$, respectively. This renormalization is caused by the local part of the interaction. Therefore we introduce a 3D-PAM, in which the f-band dispersion and the hybridization term are renormalized *ab initio* due to the local part of the interaction. We calculate $\tilde{\Sigma}(\boldsymbol{k}, \omega)$ and $\tilde{G}(\boldsymbol{k}, \omega)$ within the Matsubara frequency formalism based on the renormalized 3D-PAM. We adopt the fluctuation exchange (FLEX) approximation for calculating $\tilde{\Sigma}(\boldsymbol{k}, \omega)$.

The Hamiltonian for the renormalized 3D-PAM is expressed as follows:

$$H = H_0 + H', \tag{3}$$

$$H_0 = \sum_{\boldsymbol{k},\sigma}\left[\tilde{E}^{\mathrm{f}}_{\boldsymbol{k}} f^{\dagger}_{\boldsymbol{k}\sigma} f_{\boldsymbol{k}\sigma} + \varepsilon^{\mathrm{c}}_{\boldsymbol{k}} c^{\dagger}_{\boldsymbol{k}\sigma} c_{\boldsymbol{k}\sigma} + \tilde{V}_{\boldsymbol{k}}\left(f^{\dagger}_{\boldsymbol{k}\sigma} c_{\boldsymbol{k}\sigma} + c^{\dagger}_{\boldsymbol{k}\sigma} f_{\boldsymbol{k}\sigma}\right)\right], \tag{4}$$

$$H' = \frac{\tilde{U}}{N}\sum_{\boldsymbol{k},\boldsymbol{k}'} f^{\dagger}_{\boldsymbol{k}\uparrow} f^{\dagger}_{\boldsymbol{q}-\boldsymbol{k}\downarrow} f_{\boldsymbol{q}-\boldsymbol{k}'\uparrow} f_{\boldsymbol{k}'\downarrow}, \tag{5}$$

where $\tilde{U}$, $\tilde{E}^{\mathrm{f}}_{\boldsymbol{k}}$ and $\tilde{V}_{\boldsymbol{k}}$ are the renormalized Coulomb repulsion, the renormalized dispersion of the f-band and the renormalized hybridization term, respectively. H_0 is the unperturbed Hamiltonian and H' is the perturbation term due to the Coulomb repulsion between the f-electrons.

$\tilde{E}^{\mathrm{f}}_{\boldsymbol{k}}$ and $\tilde{V}_{\boldsymbol{k}}$ are related to the dispersion of the original f-band $\varepsilon^{\mathrm{f}}_{\boldsymbol{k}0}$ and the original hybridization term $V_{\boldsymbol{k}}$, respectively:

$$\tilde{E}^{\mathrm{f}}_{\boldsymbol{k}} = z_0\varepsilon^{\mathrm{f}}_{\boldsymbol{k}0}, \tag{6}$$

$$\tilde{V}_{\boldsymbol{k}} = \sqrt{z_0}V_{\boldsymbol{k}}. \tag{7}$$

$\mathrm{Re}\,\Sigma_{\mathrm{loc}}(\omega = 0)$ does not appear in (6) since it is included in the chemical potential of the f-band. In contrast to the f-band and the hybridization term, the conduction band is not renormalized, since only the interaction between f-electrons is considered. $V_{\boldsymbol{k}}$, $\varepsilon^{\mathrm{f}}_{\boldsymbol{k}0}$, and $\varepsilon^{\mathrm{c}}_{\boldsymbol{k}}$ are determined from the comparison with the band calculations.

Added to the f-band dispersion and the hybridization term, the Coulomb repulsion term is also renormalized:

$$\tilde{U} = z_0 U. \tag{8}$$

This result originates from the enhancement of the vertex $\Gamma = U/z_0$ and the renormalization of the interaction $\tilde{U} = z_0\Gamma z_0$ [20, 34]. According to (6) and (8), the f-band dispersion and the Coulomb repulsion term are renormalized by the same factor z_0. This indicates that $\tilde{U}/\tilde{W}_{\mathrm{f}}$ is equal to U/W_{f}, where W_{f} and $\tilde{W}_{\mathrm{f}}$ are the unrenormalized and the renormalized f-bandwidth, respectively. In this paper, we separate the effect of the electron correlation for $CeMIn_5$ into the local part and the momentum-dependent part. The local part gives rise to the local renormalization factor z_0. On the other hand, the strength of the anisotropic part is determined by $\tilde{U}/\tilde{W}_{\mathrm{f}}$, which is equal to U/W_{f}. Therefore we stress that the strength of the anisotropic part is unchanged by the local renormalization.

In order to reproduce correctly the superconducting properties for $CeMIn_5$, we have to calculate self-consistently all the parameters including T_{c}, the total mass enhancement factor, z_0 and $\tilde{U}$ from the band structure and the original Coulomb interaction U. This is because z_0

and $\tilde{U}$ are determined by the isotropic and the anisotropic part of the interaction, respectively. However, the self-consistent calculation is quite difficult in heavy fermion systems. Therefore, we treat the isotropic and anisotropic parts of the electron correlation independently. In other words, we vary z_0 independently of U. This treatment is justified because the symmetry of the anisotropic part is different from that of the isotropic one, and the pairing interaction is determined by the anisotropic part. Thus we calculate T_c and the total mass enhancement factor with various values of z_0 and U. Note that the anisotropic part of the correlation depends strongly on the topology of the Fermi surfaces. In this model. the enhancement of the electron correlation gives rise to the decrease in z_0 and the increase in U.

Equation (3) is rewritten in the 2×2 matrix form as follows [33]:

$$\begin{aligned} H_0 &= (\, f^\dagger_{k\sigma} \quad c^\dagger_{k\sigma}\,) \begin{pmatrix} \tilde{E}^{\rm f}_k & \tilde{V}_k \\ \tilde{V}_k & \varepsilon^{\rm c}_k \end{pmatrix} \begin{pmatrix} f_{k\sigma} \\ c_{k\sigma} \end{pmatrix} \\ &= (\, f^\dagger_{k\sigma} \quad c^\dagger_{k\sigma}\,) \begin{pmatrix} c(\boldsymbol{k}) & -s(\boldsymbol{k}) \\ s(\boldsymbol{k}) & c(\boldsymbol{k}) \end{pmatrix} \begin{pmatrix} E_{1k} & 0 \\ 0 & E_{2k} \end{pmatrix} \begin{pmatrix} c(\boldsymbol{k}) & s(\boldsymbol{k}) \\ -s(\boldsymbol{k}) & c(\boldsymbol{k}) \end{pmatrix} \begin{pmatrix} f_{k\sigma} \\ c_{k\sigma} \end{pmatrix} \\ &= (\, a^\dagger_{k\sigma} \quad b^\dagger_{k\sigma}\,) \begin{pmatrix} E_{1k} & 0 \\ 0 & E_{2k} \end{pmatrix} \begin{pmatrix} a_{k\sigma} \\ b_{k\sigma} \end{pmatrix}, \end{aligned} \tag{9}$$

$$E_{\frac{1}{2}k} = \tfrac{1}{2} \left\{ \varepsilon^{\rm c}_k + \tilde{E}^{\rm f}_k \pm [(\tilde{E}^{\rm f}_k - \varepsilon^{\rm c}_k)^2 + 4\tilde{V}^2_k]^{\frac{1}{2}} \right\}, \tag{10}$$

where $f_{k\sigma}(f^\dagger_{k\sigma})$, $c_{k\sigma}(c^\dagger_{k\sigma})$, $a_{k\sigma}(a^\dagger_{k\sigma})$ and $b_{k\sigma}(b^\dagger_{k\sigma})$ are the annihilation (creation) operators of the f-band, the conduction band, band 1 and band 2, respectively. $c(\boldsymbol{k})$ and $s(\boldsymbol{k})$ are defined as

$$c(\boldsymbol{k}) = \left\{ \frac{1}{2} + \frac{\tilde{E}^{\rm f}_k - \varepsilon^{\rm c}_k}{2[(\tilde{E}^{\rm f}_k - \varepsilon^{\rm c}_k)^2 + 4\tilde{V}^2_k]^{\frac{1}{2}}} \right\}^{\frac{1}{2}}, \tag{11}$$

$$s(\boldsymbol{k}) = \left\{ \frac{1}{2} - \frac{\tilde{E}^{\rm f}_k - \varepsilon^{\rm c}_k}{2[(\tilde{E}^{\rm f}_k - \varepsilon^{\rm c}_k)^2 + 4\tilde{V}^2_k]^{\frac{1}{2}}} \right\}^{\frac{1}{2}}. \tag{12}$$

In (9), the renormalized f-band and the conduction band are hybridized by $\tilde{V}_k$, following which they are diagonalized into two bands: band 1 and band 2. E_{1k} and E_{2k} denote the dispersions of band 1 and band 2, respectively ($E_{1k} > E_{2k}$).

$\varepsilon^{\rm f}_{k0}$, $\varepsilon^{\rm c}_k$ and V_k are determined such that the Fermi surfaces of band 1 and band 2 reproduce the Fermi surfaces of the 15th band and the 14th band in the band calculations, respectively. The 14th band has the largest Fermi surface, and is denoted as the β-band in the de Haas–van Alphen experiments [24–28]. On the other hand, the 15th band is denoted as the α-band, and has a smaller Fermi surface than the 14th band. $\varepsilon^{\rm f}_{k0}$ is given as follows:

$$\begin{aligned} \varepsilon^{\rm f}_{k0} = {} & \mu_{\rm f} + 2t_{\rm f1}(\cos k_{\rm a} + \cos k_{\rm b}) + 4t_{\rm f2} \cos k_{\rm a} \cos k_{\rm b} + 2t_{\rm f3}(\cos 2k_{\rm a} + \cos 2k_{\rm b}) \\ & + \cos k_{\rm c}[t_{\rm f4} + 2t_{\rm f5}(\cos k_{\rm a} \cos k_{\rm b}) + 4t_{\rm f6} \cos k_{\rm a} \cos k_{\rm b} + 2t_{\rm f7}(\cos 2k_{\rm a} + \cos 2k_{\rm b})], \end{aligned} \tag{13}$$

where $\mu_{\rm f} = 0.00$, $t_{\rm f1} = 0.43$, $t_{\rm f2} = -0.06$, $t_{\rm f3} = 0.06$, $t_{\rm f4} = -0.1$, $t_{\rm f5} = -0.06$, $t_{\rm f6} = -0.06$ and $t_{\rm f7} = 0.06$. Next, $\varepsilon^{\rm c}_k$ is expressed as follows:

$$\begin{aligned} \varepsilon^{\rm c}_k = {} & \mu_{\rm c} + 2t_{\rm c1}(\cos k_{\rm a} + \cos k_{\rm b}) + 4t_{\rm c2} \cos k_{\rm a} \cos k_{\rm b} + 2t_{\rm c3}(\cos 2k_{\rm a} + \cos 2k_{\rm b}) \\ & + \cos k_{\rm c}[t_{\rm c4} + 2t_{\rm c5}(\cos k_{\rm a} + \cos k_{\rm b}) \\ & + 4t_{\rm c6} \cos k_{\rm a} \cos k_{\rm b} + 2t_{\rm c7}(\cos 2k_{\rm a} + \cos 2k_{\rm b})]. \end{aligned} \tag{14}$$

Here, we fix $\mu_{\rm c} = -0.70$, $t_{\rm c1} = 1.00$, $t_{\rm c2} = -0.60$, $t_{\rm c3} = 0.48$, $t_{\rm c4} = -0.3$, $t_{\rm c5} = 0.0$, $t_{\rm c6} = -0.4$, and $t_{\rm c7} = 0.52$. Finally, we determine V_k as follows:

$$V_{\boldsymbol{k}} = t_{\mathrm{v}0} + 2t_{\mathrm{v}1}(\cos k_{\mathrm{a}} + \cos k_{\mathrm{b}}) + 4t_{\mathrm{v}2}\cos k_{\mathrm{a}}\cos k_{\mathrm{b}} + \cos k_{\mathrm{c}}(t_{\mathrm{v}3} + 2t_{\mathrm{v}4}(\cos k_{\mathrm{a}} + \cos k_{\mathrm{b}}) + 4t_{\mathrm{v}5}\cos k_{\mathrm{a}}\cos k_{\mathrm{b}}), \tag{15}$$

with $t_{\mathrm{v}0} = 0.30$, $t_{\mathrm{v}1} = 0.23$, $t_{\mathrm{v}2} = 0.038$, $t_{\mathrm{v}3} = 0.30$, $t_{\mathrm{v}4} = -0.23$ and $t_{\mathrm{v}5} = -0.038$.

In (13), (14) and (15), the $k_{\mathrm{a}}k_{\mathrm{b}}$-plane corresponds to the basal plane and k_{c} is a component of the wavevector perpendicular to the basal plane in $CeMIn_5$. $t_{\mathrm{f}1}$–$t_{\mathrm{f}7}$ and $t_{\mathrm{c}1}$–$t_{\mathrm{c}7}$ are the transfer integrals of the electrons occupying the f-band and the conduction band, respectively. $t_{\mathrm{v}0}$–$t_{\mathrm{v}5}$ are the hybridization term parameters. μ_{f} and μ_{c} are the chemical potentials of the f-band and the conduction band, respectively. We set $t_{\mathrm{c}1} = 1$; this is referred to as the energy unit hereafter. Comparing the obtained bands with the result of the band calculations, we determine that $t_{\mathrm{c}1}$ corresponds to a temperature of around 3000–4000 K. We assert that this model reproduces the result of the band calculations with regard to the electronic structure near the Fermi level. Hereafter, we fix $\varepsilon^{\mathrm{f}}_{\boldsymbol{k}0}$, $\varepsilon^{\mathrm{c}}_{\boldsymbol{k}}$ and $V_{\boldsymbol{k}}$ and vary U and z_0.

3. Numerical calculation by FLEX

We divide the first Brillouin zone into 64×64 meshes in the $k_{\mathrm{a}}k_{\mathrm{b}}$-plane and 32 meshes in the k_{c}-direction. We consider 2048 Matsubara frequencies. For simplicity, we hereafter abbreviate the tildes on the renormalized Green's function and self-energy term.

The dressed Green's function $\hat{G}(k)$ is expressed as the following:

$$\hat{G}(k) = \hat{G}_0(k) + \hat{G}_0(k)\hat{\Sigma}(k)\hat{G}(k), \tag{16}$$

with

$$\hat{G}(k) = \begin{pmatrix} G^{\mathrm{f}}(k) & G^{\mathrm{fc}}(k) \\ G^{\mathrm{cf}}(k) & G^{\mathrm{c}}(k) \end{pmatrix}, \tag{17}$$

$$\hat{\Sigma}(k) = \begin{pmatrix} \Sigma^{\mathrm{f}}_n(k) - \delta\mu & 0 \\ 0 & 0 \end{pmatrix}. \tag{18}$$

$\hat{G}_0(k)$ is defined as follows:

$$\hat{G}_0(k) = \begin{pmatrix} G^{\mathrm{f}}_0(k) & G^{\mathrm{fc}}_0(k) \\ G^{\mathrm{cf}}_0(k) & G^{\mathrm{c}}_0(k) \end{pmatrix} = \begin{pmatrix} c^2G_1(k) + s^2G_2(k) & sc(G_1(k) - G_2(k)) \\ sc(G_1(k) - G_2(k)) & s^2G_1(k) + c^2G_2(k) \end{pmatrix}, \tag{19}$$

where

$$G_{\frac{1}{2}}(k) = \frac{1}{\mathrm{i}\varepsilon_m - E_{\frac{1}{2}\boldsymbol{k}}}. \tag{20}$$

In (20), $\varepsilon_m = (2m+1)\pi T$ is a fermion Matsubara frequency. The shift in chemical potential $\delta\mu$ is determined by the conservation of the total electron number:

$$\sum_k \left(G^{\mathrm{f}}(k) + G^{\mathrm{c}}(k) - G^{\mathrm{f}}_0(k) - G^{\mathrm{c}}_0(k)\right) = 0. \tag{21}$$

In (18), the self-energy correction term appears only in the f-electron component. This is because electron correlation is taken into account only among f-electrons.

In order to consider the effect of the anisotropic part of the interaction, we need to approximate the non-local part of the self-energy terms. From the various methods available for approximation, we adopt the FLEX approximation [36–39, 21] in this paper. This is because

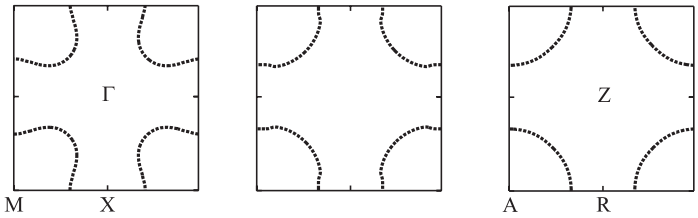

Figure 1. The Fermi surface of band 1. The figures on the left, middle and right correspond to $k_c = 0$, $k_c = \pi/2$ and $k_c = \pi$, respectively. U, z_0 and T are fixed at 2.10, 0.12 and 0.000 48, respectively.

FLEX reproduces well the characteristics of strong AF fluctuation systems. In the FLEX approximation, the non-local normal self-energy term $\Sigma_n^{\mathrm{f}}(k)$ is written as follows:

$$\Sigma_n^{\mathrm{f}}(k) = \frac{T}{N}\sum_q V(q)G^{\mathrm{f}}(k-q), \tag{22}$$

$$V(q) = \frac{3}{2}\tilde{U}^2\frac{\tilde{\chi}(q)}{1-\tilde{U}\tilde{\chi}(q)} + \frac{1}{2}\tilde{U}^2\frac{\tilde{\chi}(q)}{1+\tilde{U}\tilde{\chi}(q)} - \tilde{U}^2\tilde{\chi}(q). \tag{23}$$

Hereafter, $(\boldsymbol{k}, \varepsilon_n)$ and $(\boldsymbol{q}, \omega_n)$ are abbreviated as k and q, respectively. Here, $\omega_m = 2m\pi T$ is a boson Matsubara frequency. In (23), $\tilde{\chi}(q)$ is the renormalized spin susceptibility and is defined as follows:

$$\tilde{\chi}(q) = -\frac{T}{N}\sum_q G^{\mathrm{f}}(k+q)G^{\mathrm{f}}(k). \tag{24}$$

With increasing $\tilde{U}$, $\tilde{U}\tilde{\chi}_{\max}(q)$ increases. Here $\tilde{\chi}_{\max}(q)$ is the maximum value of $\tilde{\chi}(q)$. Equation (23) shows that $V(q)$ diverges when $\tilde{U}\tilde{\chi}_{\max}(q)$ reaches unity. This corresponds to an antiferromagnetic (AF) transition. However, it is difficult to calculate the self-energy term for $\tilde{U}\tilde{\chi}_{\max}(q) \to 1$. Therefore, we assume U_{AF} as the value of U when $\tilde{U}\tilde{\chi}_{\max}(q)$ reaches 0.998.

Figures 1 and 2 show the Fermi surfaces of bands 1 and 2, respectively. It is indicated from the calculation that the Fermi surfaces are nearly unchanged as a function of z_0 and of U, with $\varepsilon_{k0}^{\mathrm{f}}$, $\varepsilon_k^{\mathrm{c}}$ and V_k fixed. The band structure and the density of states (DOS) for the f-band are plotted in figures 3 and 4, respectively. The DOS of the f-band $\rho_{\mathrm{f}}(\varepsilon)$ is given by

$$\rho_{\mathrm{f}}(\varepsilon) = -\frac{1}{\pi}\mathrm{Im}\sum_{\boldsymbol{k}} G^{\mathrm{fR}}(\boldsymbol{k}, \varepsilon). \tag{25}$$

Here, $G^{\mathrm{fR}}(\boldsymbol{k}, \varepsilon)$ is obtained by the analytic continuation $\mathrm{i}\varepsilon_n \to \varepsilon$ from $G^{\mathrm{f}}(k)$. It is indicated from the calculation that the DOS at the Fermi level is nearly unchanged as a function of U, with $\varepsilon_{k0}^{\mathrm{f}}$, $\varepsilon_k^{\mathrm{c}}$ and V_k fixed. On the other hand, the DOS varies in inverse proportion to z_0.

Next, we calculate T_{c} by solving the linearized Dyson–Gor'kov equation [37–39]. First of all, the normal and anomalous Green's functions satisfy Dyson–Gor'kov equations [33]:

$$G^{\mathrm{f}}(k) = G_0^{\mathrm{f}}(k) + G_0^{\mathrm{f}}(k)\Sigma_n^{\mathrm{f}}(k)G^{\mathrm{f}}(k) + G_0^{\mathrm{f}}(k)\Sigma_a(k)F^{\dagger}(k), \tag{26}$$

$$F^{\dagger}(k) = G_0^{\mathrm{f}}(-k)\Sigma_n^{\mathrm{f}}(-k)F^{\dagger}(k) + G_0^{\mathrm{f}}(-k)\Sigma_a(-k)G^{\mathrm{f}}(k). \tag{27}$$

Approaching T_{c} within the superconducting state, (26) and (27) are linearized as follows:

$$F(k) = \left|G^{\mathrm{f}}(k)\right|^2\Sigma_a(k), \tag{28}$$

$$G^{\mathrm{f}}(k) = G_0^{\mathrm{f}}(k) + G_0^{\mathrm{f}}(k)\Sigma_n^{\mathrm{f}}(k)G^{\mathrm{f}}(k). \tag{29}$$

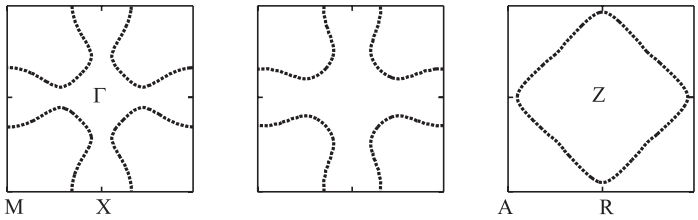

Figure 2. The Fermi surface of band 2. The figures on the left, middle and right correspond to $k_c = 0$, $k_c = \pi/2$ and $k_c = \pi$, respectively. U, z_0 and T are fixed at 2.10, 0.12 and 0.000 48, respectively.

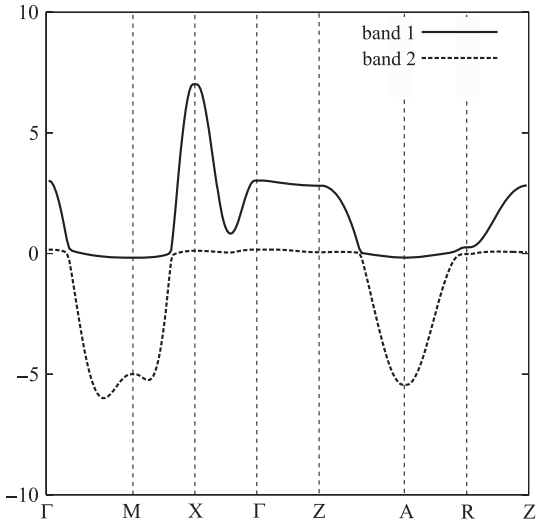

Figure 3. The band structure with $U = 2.10$, $z_0 = 0.12$ and $T = 0.000\,48$, respectively. The solid and dashed curves correspond to band 1 and band 2, respectively.

The self-energy correction affects only the f-electrons. As a result, we need to consider only the f-electron Green's functions. Therefore, we consider only the f-band component of the Green's function and the self-energy term. In the linearized Dyson–Gor'kov equation, the anomalous self-energy term $\Sigma_a(k)$ is expressed as follows:

$$\Sigma_a(k) = -\frac{T}{N}\sum_{k'} V_a(q)|G^{\mathrm{f}}(k-q)|^2\Sigma_a(k-q), \tag{30}$$

$$V_a(q) = \tilde{U}^2\left(\frac{3}{2}\frac{\tilde{\chi}(q)}{1-\tilde{U}\tilde{\chi}(q)} - \frac{1}{2}\frac{\tilde{\chi}(q)}{1+\tilde{U}\tilde{\chi}(q)}\right) + \tilde{U}. \tag{31}$$

If we replace the left-hand side of (30) by $\lambda\Sigma_a(k)$, it can be considered as an eigenvalue equation with the eigenvalue λ and the eigenvector $\Sigma_a(k)$. Here, the eigenvalues for $\mathrm{d}_{x^2-y^2}$ and d_{xy} pairing symmetries are denoted as $\lambda_{x^2-y^2}$ and λ_{xy}, respectively. The eigenvalues $\lambda_{x^2-y^2}$ and λ_{xy} are obtained by calculating (30) self-consistently, using the initial values of $\Sigma_a(k) \propto \cos k_a - \cos k_b$ and $\sin k_a \sin k_b$, respectively.

Figure 5 shows $\lambda_{x^2-y^2}$ for various values of U for $z_0 = 0.12$ and $T = 0.000\,48$. According to the result, $\lambda_{x^2-y^2}$ reaches unity with $U \sim 1.96$. On the other hand, a positive value is not obtained for λ_{xy} from the calculation. This indicates that the d_{xy} pairing state

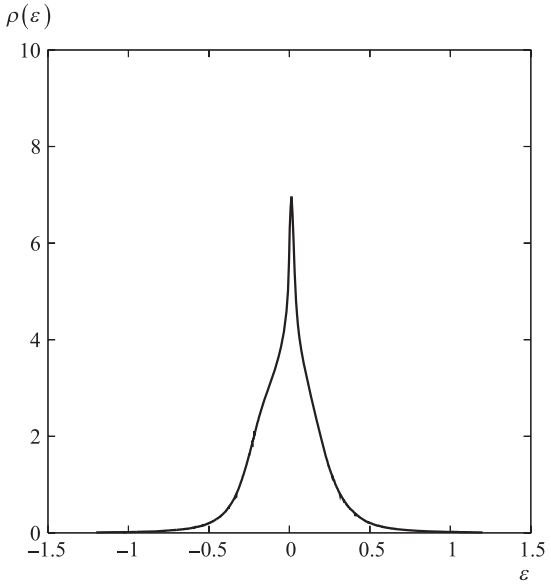

Figure 4. The DOS of the f-band with $U = 2.10$, $z_0 = 0.12$ and $T = 0.000\,48$.

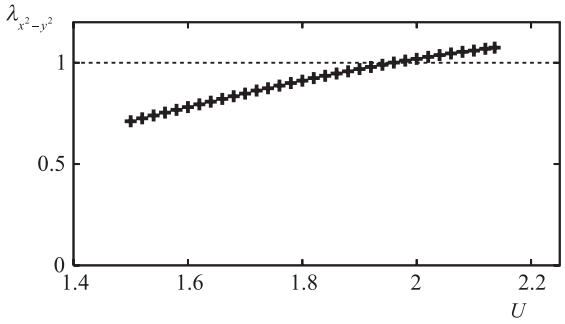

Figure 5. $\lambda_{x^2-y^2}$ is plotted. z_0 and T are fixed at 0.12 and 0.000 48, respectively. λ_{xy} is not plotted, since a positive value is not obtained.

is never realized in $CeMIn_5$. In fact, the $d_{x^2-y^2}$ state possesses the maximum eigenvalue among the gap symmetries. This fact indicates that $d_{x^2-y^2}$ pairing symmetry is actually realized in superconducting $CeMIn_5$. This is considered to result from the AF fluctuation. The susceptibility $\tilde{\chi}(\boldsymbol{q}, \omega_0)$ is plotted in figure 6. Figure 6 indicates that $\tilde{\chi}(\boldsymbol{q}, \omega_0)$ has a peak at the M-point, that is, $\boldsymbol{q} = (\pi, \pi, 0)$. This suggests the existence of AF fluctuation. This is consistent with experiments, such as NQR measurement.

T_c is the temperature at which $\lambda_{x^2-y^2}$ reaches unity. The calculated T_c for $d_{x^2-y^2}$ symmetry is plotted in figures 7 and 8. Figure 7 shows the U-dependence of T_c with z_0 fixed to 0.12. Figure 7 indicates that T_c increases with the increase in U. On the other hand, figure 8 shows the z_0-dependence of T_c with U fixed to 2.10. It is indicated that T_c increases approximately in proportion to z_0.

The behaviour of T_c is explained as follows. When U is fixed, $\tilde{W}_f$ and $\tilde{U}$ vary approximately in proportion to z_0. Moreover, the Fermi surface is nearly unchanged with the variation of z_0. It is considered that z_0 affects T_c by scaling the energy [31]. Therefore,

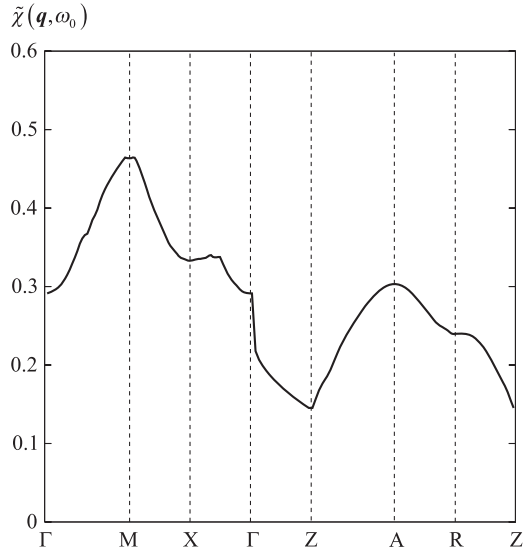

Figure 6. The susceptibility $\tilde{\chi}(\boldsymbol{q}, \omega_0)$ is plotted. U, z_0 and T are fixed at 2.10, 0.12 and 0.000 48, respectively. $\tilde{\chi}(\boldsymbol{q}, \omega_0)$ has a peak at the M-point, that is, $\boldsymbol{q} = (\pi, \pi, 0)$. This corresponds to AF fluctuation.

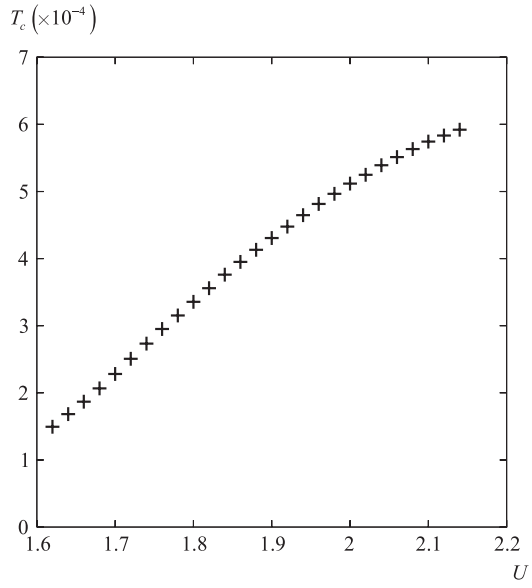

Figure 7. U-dependence of T_c for $d_{x^2-y^2}$ symmetry is plotted. z_0 is fixed at 0.12. At $U = 2.159$, the system exhibits AF transition.

T_c varies in proportion to z_0. On the other hand, the pairing symmetry is determined mainly by the momentum-dependent parts of the interaction, especially by the topology of the Fermi surfaces. T_c is determined by the strength of the anisotropic part of the correlation: however, it does not account for the energy-scaling factor arising from the local renormalization factor z_0. In our model, the strength of the anisotropic part is determined by $\tilde{U}/\tilde{W}_f$. $\tilde{U}/\tilde{W}_f$ is equal

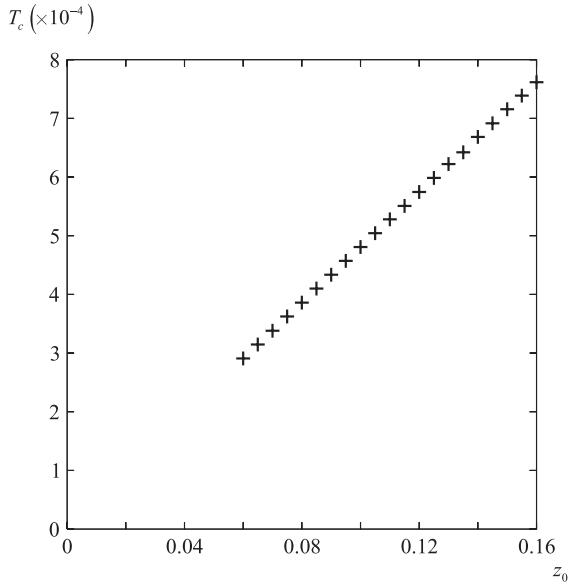

Figure 8. The dependence of T_c on z_0 is shown. T_c varies proportionally to z_0, due to the energy scaling. U is fixed at 2.10.

to U/W_f. Here, the unrenormalized f-bandwidth W_f is fixed in this paper, since ε^f_{k0} is fixed. Therefore, we can treat U as the parameter for the strength of the anisotropic part. As a result, T_c is affected by U through the non-local part of the quasiparticle interaction, and scaled by z_0 through the local renormalization.

Next, we investigate the total mass enhancement factor for the f-band. The total mass enhancement factor is defined as the inverse of the total wavefunction renormalization factor and is expressed as follows:

$$z_{tot}(\boldsymbol{k})^{-1} = z^{-1}(\boldsymbol{k}) z_0^{-1}, \tag{32}$$

where the non-local mass enhancement factor $z^{-1}(\boldsymbol{k})$ is defined as $z^{-1}(\boldsymbol{k}) = 1 - \partial \mathrm{Re}\Sigma^R_n(\boldsymbol{k}, \varepsilon)/\partial\varepsilon|_{\varepsilon=0}$. We define z^{-1}_{tot} as the average of $z^{-1}_{tot}(\boldsymbol{k})$ over the k-space. Hereafter, we denote z^{-1}_{tot} as the total mass enhancement factor.

Figures 9 and 10 show the dependences of z^{-1}_{tot} on z_0 and U, respectively. Figure 9 shows that z^{-1}_{tot} decreases in inverse proportion to increasing z_0. This is because the Coulomb repulsion term and the f-band dispersion are renormalized by the same factor z_0, and therefore $z^{-1}(\boldsymbol{k})$ is nearly unchanged with varying z_0. On the other hand, z^{-1}_{tot} increases with the increase in U. This is due to the increase in $z^{-1}(\boldsymbol{k})$, which is generally observed in PAM and the Hubbard model.

Next, we consider fitting the parameters U and z_0 in our model. We cannot necessarily equate the measured cyclotron mass of the α- and β-band to the calculated value of z^{-1}_{tot} in our model. Nevertheless, it is considered that the measured cyclotron mass and z^{-1}_{tot} are of the same order. The cyclotron masses of the α- and β-bands for $CeCoIn_5$ are approximately 15 and 60, respectively, at ambient pressure [27]. Therefore we assume z^{-1}_{tot} to be 30, which is the geometric mean of the cyclotron mass of the α- and β-bands.

According to figures 7–10, T_c and z^{-1}_{tot} for $U = 2.12$ and $z_0 = 0.12$ is approximately 0.0006 and 30, respectively. Since t_{c1} is of the order of 3000–4000 K, the calculated T_c is approximately 2 K, which coincides approximately with the measured T_c for $CeCoIn_5$ at

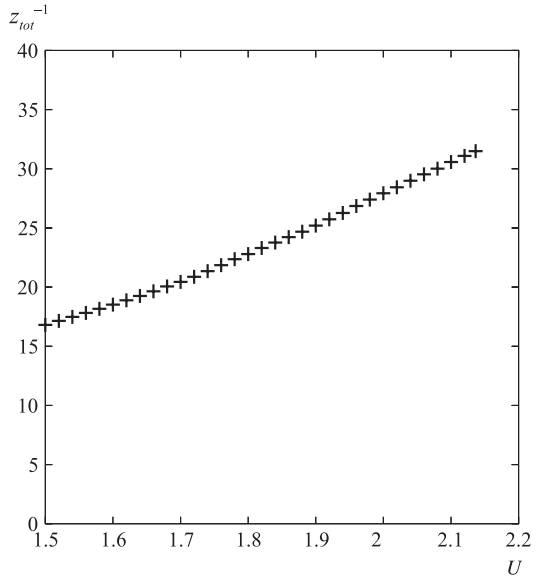

Figure 9. The dependence of $z_{\rm tot}^{-1}$ on U with z_0 and T fixed at 2.10, 0.12 and 0.000 48, respectively. $z_{\rm tot}^{-1}$ increases with the increase in U.

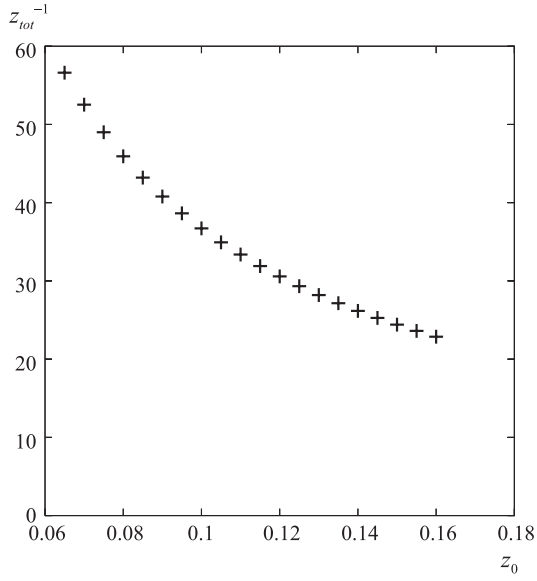

Figure 10. The dependence of $z_{\rm tot}^{-1}$ on z_0 with U and T fixed at 2.10 and 0.000 48, respectively. $z_{\rm tot}^{-1}$ varies in inverse proportion to z_0.

ambient pressure. Therefore, we assume that $U = 2.12$ and $z_0 = 0.12$ for $CeCoIn_5$, since T_c and the mass enhancement factor are reproduced well. We can fit the parameters for $CeIrIn_5$ similarly. For $CeIrIn_5$ with $T_c = 0.4$ K, we estimate T_c and $z_{\rm tot}^{-1}$ at 0.000 12 and 20, respectively. We obtain $U = 1.61$ and $z_0 = 0.110$ for $CeIrIn_5$, which give rise to the estimated value for T_c and $z_{\rm tot}^{-1}$.

Finally in this section, we discuss the efficiency of the application of FLEX to our model. It is certain that the FLEX treatment does not reproduce the correct Kondo scale. However, it is considered that $CeMIn_5$ is near the antiferromagnetic quantum critical point (AF-QCP) and is not strongly Kondo-like. Moreover, the local part of the correlation, which contributes to the Kondo scaling, does not affect the pairing interaction for anisotropic superconductivity. In our model, the local part of the electron correlation is taken into account by introducing the local renormalization factor z_0. This renormalization procedure corresponds to the so-called Kondo scaling in the case of a single impurity. As a conclusion, AF fluctuation plays a far more important role in the superconductivity for $CeMIn_5$ than the local part of the electron correlation. Therefore, the application of FLEX to our model is efficient and reliable for discussing the superconductivity of $CeMIn_5$.

4. Behaviour of $CeMIn_5$ under hydrostatic pressure

The physical properties of $CeMIn_5$ are sensitive to pressure. For $CeCoIn_5$, Δ_0/k_BT_c decreases from a value greater than 4 at ambient pressure to a value lower than 3 at 2 GPa [6, 7]. In the vicinity of ambient pressure, the decrease of Δ_0/k_BT_c is quite moderate, while Δ_0/k_BT_c decreases markedly under higher pressure ($\sim$1 GPa). Analogous pressure dependence is observed in $\Delta C/\gamma T_c$ for $CeCoIn_5$, where ΔC is the specific heat jump at the superconducting transition [40, 41]. In the Shubnikov–de Haas experiment for $CeCoIn_5$, the cyclotron masses for the α- and β-band reduce monotonically with the increase in pressure [27]. A decrease in C/T up to 1.5 GPa is reported [40]. The decrease in C/T indicates the reduction in the mass enhancement factor or the expansion of the bandwidth, since C/T is approximately proportional to the DOS at the Fermi level. Although marked changes in the physical properties are caused by pressure, the de Haas–van Alphen frequency is nearly unchanged from ambient pressure up to 3 GPa for $CeCoIn_5$ [27]. This indicates that the Fermi surfaces of $CeCoIn_5$ remain unchanged under pressure.

On the other hand, the ratio Δ_0/k_BT_c in $CeIrIn_5$ remains nearly constant at approximately 2.5 from ambient pressure up to 2 GPa [9]. With regard to the specific heat measurements, C/T decreases monotonically up to 2 GPa [42]. A similar pressure dependence is observed for $(1/T_1T)^{\frac{1}{2}}$ for the normal state under pressures greater than 1 GPa, where AF fluctuation is weak [9].

The measurements of Δ_0/k_BT_c indicate that the superconductivity for $CeCoIn_5$ changes from a strong coupling superconductivity at ambient pressure to an ordinary one at high pressure, while the superconductivity for $CeIrIn_5$ is an ordinary one. Based on these facts, we assume that the electron correlation reduces with the increase in pressure for $CeCoIn_5$. On the other hand, we assume that the correlation is not strong at ambient pressure and the reduction in the correlation with the increase in pressure is considerably small for $CeIrIn_5$, as compared with the case for $CeCoIn_5$.

Moreover, a difference in the pressure dependence of T_c of $CeIrIn_5$ and $CeCoIn_5$ is observed. For $CeCoIn_5$ [23], T_c increases slightly with increase in pressure up to 1 GPa. Under pressures greater than 1 GPa, T_c decreases sharply. For $CeIrIn_5$, T_c increases with increase in pressure up to 3 GPa [9, 43]. The pressure at which T_c reaches the maximum is approximately 1 GPa and 3 GPa for $CeCoIn_5$ [23] and $CeIrIn_5$ [43], respectively. Note that the increase in T_c from ambient pressure to its maximum is considerably larger in $CeIrIn_5$ than in $CeCoIn_5$.

5. Behaviour of $CeMIn_5$ under hydrostatic pressure: calculation

With the increase in pressure, the bandwidth of the f-band and that of the conduction band is expanded due to compression. Moreover, the original hybridization term V_k changes under pressure. As a matter of fact, the change in the band structure under pressure is considered to be

quite complicated. However, the effect of the pressure on PAM is considered to be reproduced by the reduction in the electron correlation. In the renormalized 3D-PAM, the reduction in the electron correlation corresponds to the increase in z_0 and/or the decrease in U. Here, note that the expansion in the bandwidth of the f-band also increases the energy scale. We include this effect in the increase in z_0, and assume $\varepsilon^{\mathrm{f}}_{\boldsymbol{k}0}$ to be unchanged. As a conclusion, we assert that the increase in pressure corresponds to the decrease in U and/or the increase in z_0. Here, we assume that $\varepsilon^{\mathrm{f}}_{\boldsymbol{k}0}$, $\varepsilon^{\mathrm{c}}_{\boldsymbol{k}}$ and $V_{\boldsymbol{k}}$ are fixed. This treatment is justified since Fermi surfaces remain nearly unchanged under pressure.

Next, we estimate the variation of U and z_0 under pressure. In the calculation using Hubbard model it is indicated that $\Delta_0/k_{\mathrm{B}}T_{\mathrm{c}}$ and $\Delta C/\gamma T_{\mathrm{c}}$ increase with the increase in U [21]. Since $\Delta_0/k_{\mathrm{B}}T_{\mathrm{c}}$ and $\Delta C/\gamma T_{\mathrm{c}}$ are not affected by energy scaling in our model, we can assume that z_0 does not affect $\Delta_0/k_{\mathrm{B}}T_{\mathrm{c}}$ or $\Delta C/\gamma T_{\mathrm{c}}$. Therefore, $\Delta_0/k_{\mathrm{B}}T_{\mathrm{c}}$ and $\Delta C/\gamma T_{\mathrm{c}}$ are determined mainly by U, according to the analogy to the case in the Hubbard model [21]. This suggests that we can estimate the variation of U from the variation of $\Delta_0/k_{\mathrm{B}}T_{\mathrm{c}}$ and of $\Delta C/\gamma T_{\mathrm{c}}$. Then, we discuss C/T and $(1/T_1T)^{\frac{1}{2}}$. C/T is approximately proportional to the DOS at the Fermi level. Ignoring the effect of AF fluctuation, $(1/T_1T)^{\frac{1}{2}}$ is also proportional to the DOS. In our model, the DOS at the Fermi level is not affected by U, and varies in inverse proportion to z_0. Therefore, it is considered that C/T and $(1/T_1T)^{\frac{1}{2}}$ vary in inverse proportion to z_0.

According to $\Delta_0/k_{\mathrm{B}}T_{\mathrm{c}}$ and $\Delta C/\gamma T_{\mathrm{c}}$, we can assume that U decreases moderately with the increase in pressure under low pressure, and that U decreases sharply under high pressure for $CeCoIn_5$. For $CeIrIn_5$, it is considered that U is nearly unchanged under pressure up to 2 GPa. On the other hand, we assume that z_0 increases with the increase in pressure up to 2 GPa for $CeIrIn_5$.

Based on the above discussions, we explain the pressure dependence of T_{c} and cyclotron mass. First, we discuss $CeCoIn_5$. If we assume that z_0 increases with the increase in pressure obeying the C/T measurements [40], we can explain the pressure dependence of T_{c} for $CeCoIn_5$ qualitatively. As plotted in figures 7 and 8, pressure affects T_{c} as follows: the decrease in U gives rise to the decrease in T_{c}, and the increase in z_0 gives rise to the increase in T_{c}. The pressure dependence of T_{c} is determined by which effect, decrease in U or increase in z_0, is dominant. In the low-pressure region, the effect of the increase in z_0 is dominant since the decrease in U is moderate. Therefore, T_{c} increases slightly with the increase in pressure. On the other hand, in the high-pressure region the effect of the decrease in U is dominant since the decrease in U is steep. Moreover, the cyclotron mass is explained by the assumed variation of U and z_0 under pressure. Both the decrease in U and the increase in z_0 give rise to the decrease in z_{tot}^{-1}, as plotted in figures 9 and 10. Therefore, we can explain that pressure reduces the cyclotron mass.

Next, we discuss T_{c} for $CeIrIn_5$ up to 2 GPa. It is considered that U remains nearly unchanged and z_0 increases with the increase in pressure. Therefore, we can explain that T_{c} for $CeIrIn_5$ increases due to the increase in z_0.

6. Conclusion

We have studied the superconductivity in $CeMIn_5$ by using the FLEX approximation on the basis of a 3D-PAM. We have confirmed that the $d_{x^2-y^2}$ pairing symmetry is realized in $CeMIn_5$ from the comparison of the eigenvalue for the Èliashberg equation. In superconducting $CeMIn_5$, the $d_{x^2-y^2}$ pairing symmetry is realized due to the AF fluctuation.

Furthermore, we have pointed out that there exist two essential parameters that determine T_{c} and total mass enhancement. One is the local wavefunction renormalization factor z_0, which scales the bandwidth of quasi-particles. The other is the Coulomb repulsion parameter U,

which affects T_c and total mass enhancement through the non-local part of the quasi-particle interaction. The non-local part of the interaction leads to anisotropic superconductivity due to the the momentum dependence of the interaction between quasi-particles. With the increase in pressure, z_0 increases and/or U decreases. In our analysis, the increase in U means an increase in the anisotropic part of the interaction and gives rise to stronger AF fluctuation. On the other hand, the decrease in z_0 corresponds to an increase in the isotropic part of the interaction. The increase in z_0 lifts T_c through the energy scaling, and the decrease in U lowers T_c through the reduced correlation. We explain the superconductivity in $CeMIn_5$ using this model, in which T_c and the mass enhancement factor coincide approximately with the experimental results.

Next, we have estimated the variation of U and z_0 under pressure. From this estimation, we have qualitatively explained the pressure dependence of T_c for $CeCoIn_5$ and $CeIrIn_5$. For $CeCoIn_5$, it is considered that both the increase in z_0 and the decrease in U are invoked by pressure. In the low-pressure region, T_c increases slightly with the increase in pressure. This is because the decrease in U is moderate and the effect of the increase in z_0 is dominant on T_c. On the other hand, T_c decreases with the increase in pressure in the high-pressure region. This is because the decrease in U is marked and dominates over the increase in z_0. For $CeIrIn_5$, it is considered that z_0 increases with the increase in pressure, while U is nearly unchanged up to 2 GPa. Therefore T_c increases monotonically with the increase in pressure, up to 2 GPa.

Acknowledgment

Numerical computation in this work was carried out with sx8 at the Yukawa Institute Computer Facility, Kyoto University.

References

[1] Petrovic C, Pagliuso P G, Hundley M F, Movshovich R, Sarrao J L, Thompson J D, Fisk Z and Monthoux P 2001 *J. Phys.: Condens. Matter* **13** L337
[2] Petrovic C, Movshovich R, Jaime M, Pagliuso P G, Hundley M F, Sarrao J L, Fisk Z and Thompson J D 2001 *Europhys. Lett.* **53** 354
[3] Hegger H, Petrovic C, Moshopoulou E G, Hundley M F, Sarrao J L, Fisk Z and Thompson J D 2000 *Phys. Rev. Lett.* **84** 4986
[4] Fisher R A, Bouquet F, Phillips N E, Hundley M F, Pagliuso P G, Sarrao J L, Fisk Z and Thompson J D 2002 *Phys. Rev.* B **65** 224509
[5] Kawasaki Y, Kawasaki S, Yashima M, Mito T, Zheng G, Kitaoka Y, Shishido H, Settai R, Haga Y and Onuki Y 2003 *J. Phys. Soc. Japan* **72** 2038
[6] Yashima M, Kawasaki S, Kawasaki Y, Zheng G, Kitaoka Y, Shishido H, Settai R, Haga Y and Onuki Y 2004 *J. Phys. Soc. Japan* **73** 2073
[7] Yashima M, Kawasaki S, Kawasaki Y, Zheng G, Kitaoka Y, Shishido H, Settai R, Haga Y and Onuki Y 2005 *Physica* B **359–361** 404
[8] Zheng G, Tanabe K, Mito T, Kawasaki S, Kitaoka Y, Aoki D, Haga Y and Onuki Y 2001 *Phys. Rev. Lett.* **86** 4664
[9] Kawasaki S, Zheng G, Kan H, Kitaoka Y, Shishido H and Onuki Y 2005 *Phys. Rev. Lett.* **94** 037007
[10] Mito T, Kawasaki S, Zheng G, Kawasaki Y, Ishida K, Kitaoka Y, Aoki D, Haga Y and Onuki Y 2001 *Phys. Rev.* B **63** 220507
[11] Movshovich R, Jaime M, Thompson J D, Petrovic C, Fisk Z, Pagliuso P G and Sarrao J L 2001 *Phys. Rev. Lett.* **86** 5152
[12] Ikeda S *et al* 2001 *J. Phys. Soc. Japan* **70** 2248
[13] Matsuda Y and Izawa K 2003 *Physica* C **388/389** 487
[14] Matsuda Y, Izawa K and Vekhter I 2006 *J. Phys.: Condens. Matter* **18** R705
[15] Matsuda Y and Izawa K 2003 *J. Low Temp. Phys.* **131** 429
[16] Izawa K, Yamaguchi H, Matsuda Y, Shishido H, Settai R and Onuki Y 2003 *Physica* C **388/389** 537
[17] Izawa K, Yamaguchi H, Matsuda Y, Shishido H, Settai R and Onuki Y 2001 *Phys. Rev. Lett.* **87** 057002

[18] Izawa K, Yamaguchi H, Matsuda Y, Sasaki T, Fukase T, Yoshida Y, Settai R and Onuki Y 2002 *Physica* C **367** 15
[19] Aoki H, Sakakibara T, Shishido H, Settai R, Onuki Y, Miranovic P and Machida K 2004 *J. Phys.: Condens. Matter* **16** L13
[20] Nisikawa Y, Ikeda H and Yamada K 2002 *J. Phys. Soc. Japan* **71** 1140
[21] Ikeda H, Nisikawa Y and Yamada K 2003 *J. Phys.: Condens. Matter* **15** S2241
[22] Maehira T, Hotta T, Ueda K and Hasegawa A 2003 *J. Phys. Soc. Japan* **72** 854
[23] Onuki Y, Settai R, Sugiyama K, Takeuchi T, Kobayashi T, Haga Y and Yamamoto E 2004 *J. Phys. Soc. Japan* **73** 769
[24] Haga Y *et al* 2001 *Phys. Rev.* B **63** 060503
[25] Hall D *et al* 2001 *Phys. Rev.* B **64** 064506
[26] Shishido H *et al* 2002 *J. Phys. Soc. Japan* **71** 162
[27] Shishido H, Ueda T, Hashimoto S, Kubo T, Settai R, Harima H and Onuki Y 2003 *J. Phys.: Condens. Matter* **15** L499
[28] Settai R, Shishido H, Ikeda S, Murakawa Y, Nakashima M, Aoki D, Haga Y, Ueda T, Harima H and Onuki Y 2001 *J. Phys.: Condens. Matter* **13** L627
[29] Ikeda H 2002 *J. Phys. Soc. Japan* **71** 1126
[30] Tanaka K, Ikeda H, Nisikawa Y and Yamada K 2006 *J. Phys. Soc. Japan* **75** 024713
[31] Shinkai S, Ikeda H and Yamada K 2006 *J. Phys. Soc. Japan* **75** 104712
[32] Yamada K and Yosida K 1986 *Prog. Theor. Phys.* **76** 321
[33] Hotta T 1994 *J. Phys. Soc. Japan* **63** 4126
[34] Hewson A C 1993 *Phys. Rev. Lett.* **70** 4007
[35] Hewson A C 1994 *Adv. Phys.* **43** 543
[36] Bickers N E, Scalapino D J and White S R 1989 *Phys. Rev. Lett.* **62** 961
[37] Kondo H and Moriya T 1998 *J. Phys. Soc. Japan* **67** 3695
[38] Kondo H and Moriya T 1999 *J. Phys. Soc. Japan* **68** 3170
[39] Kondo H and Moriya T 2004 *J. Phys. Soc. Japan* **73** 812
[40] Sparn G, Borth R, Lengyel E, Pagliuso P G, Sarrao J L, Steglich F and Thompson J D 2002 *Physica* B **319** 262
[41] Knebel G, Measson M, Salce B, Aoki D, Braithwaite D, Brison J P and Flouquet J 2004 *J. Phys.: Condens. Matter* **16** 8905
[42] Sparn G, Lengyel E, Pagliuso P G, Sarrao J L, Sparn G, Steglich F and Thompson J D 2002 *Physica* B **312** 136
[43] Muramatsu T, Kobayashi T, Shimizu K, Amaya K, Aoki D, Haga Y and Onuki Y 2003 *Physica* C **388/389** 539